ADVANCED FUNCTIONAL MATERIALS
www.afm-journal.de

Low-Cost WS_2 Photodetector on Water-Soluble Paper for Transient Electronics

Gulsum Ersu, Luke Doolan, Thomas Pucher, Jonathan N. Coleman, and Andres Castellanos-Gomez**

The rapid development of technology has led to a significant increase in the production of electronic devices, raising concerns about electronic waste (e-waste). Transient electronics, i.e., devices designed to disappear or dissolve after use. Offer a promising route to mitigate this challenge. Here, the first demonstration of a transient photodetector is reported based on direct abrasion-deposited WS_2 on water-soluble paper, using graphite electrodes drawn directly on the substrate. The whole device can physically disappear in water in ≈60 s, and the electronic materials can be recovered by vacuum filtration. The device shows a photoresponsivity of ≈176 µA W^{-1} under ambient conditions.

1. Introduction

With the accelerated development of electronics, the production of devices is rapidly scalating worldwide leading to significant amounts of electronic waste that often cannot be efficiently recycled.[1–3] Even if the degradation of standard electronic components does occur, it often results in the release of toxic materials posing significant risks to living organisms and the environment.[4]

This big problem motivated researchers and industries to not only improve recycling methods but also to create electronics with a lower environmental footprint upon end of use. Biodegradable electronics that can partially or completely degrade in nature have emerged as an essential solution to reduce environmental burdens.[5] Although long-term operation is a feature of traditional electronics, biodegradable devices can potentially offer great benefits to temporary biomedical implants, green environmental electronics, and secure hardware. Till now, a wide range of biodegradable substrates (such as paper, silk, synthetic polymers, etc.) have been reported.[6–8] Partially degradable inorganic transistors on a silk substrate were proposed the concept of transitional electronics for the first time.[9] Despite their excellent degradation capability and performance, silk electronics are highly susceptible to water and solvents. Several studies have reported depositing organic semiconductors on paper and polymeric substrates. The degradation time of these materials can be adjusted from a few days to several years, depending on specific applications. In recent studies, silicon nanomembranes have been shown to dissolve in physiological environments at a rate of a few nanometers to more than 100 nm per day, depending on the types of aqueous solutions.[10–14] However, even though they are flexible and degradable, the performance of such devices falls behind the requirements of many electronics applications.

Apart from biodegradable electronics, there are other applications that require very fast degradation after use. Transient electronics are an emerging class of functional electronic devices to operate over a short time and predefined duration of time, varying from a few minutes to days, without the need for harsh solvents.[15–17] They are designed to disintegrate, either partially or completely, through electrochemical, mechanical, or chemical reactions when no longer needed.[16,18–20] For instance, temporary implantable biomedical devices are designed to degrade in the body without requiring secondary surgery to extract the device.[21–23] The unique property of transient electronics to break down into harmless substances when triggered by environmental factors such as moisture, light, or temperature has initiated the way for research areas like eco-friendly electronics, implantable biomedical devices, hardware security, and environmental sensors.[24–28] These controlled degradable devices are promising solutions for eco-friendly and sustainable electronics.

In this study, we report the first demonstration of a WS_2 transient photodetector on water-soluble paper based on the direct abrasion of photoactive material and electrode. This fabrication approach requires no solvents, no lithography, and no energy-intensive processing, making it uniquely suited for accessible, low-impact device manufacturing. While transient electronics on water-soluble substrates are not new, previous research has

G. Ersu, T. Pucher, A. Castellanos-Gomez
2D Foundry Group
Instituto de Ciencia de Materiales de Madrid (ICMM-CSIC)
Madrid E-28049, Spain
E-mail: gulsum.ersu@icmm.csic.es; andres.castellanos@csic.es
L. Doolan, J. N. Coleman
School of Physics
CRANN and AMBER Research Centres
Trinity College Dublin
Dublin 2, Ireland

DOI: 10.1002/adfm.202509505

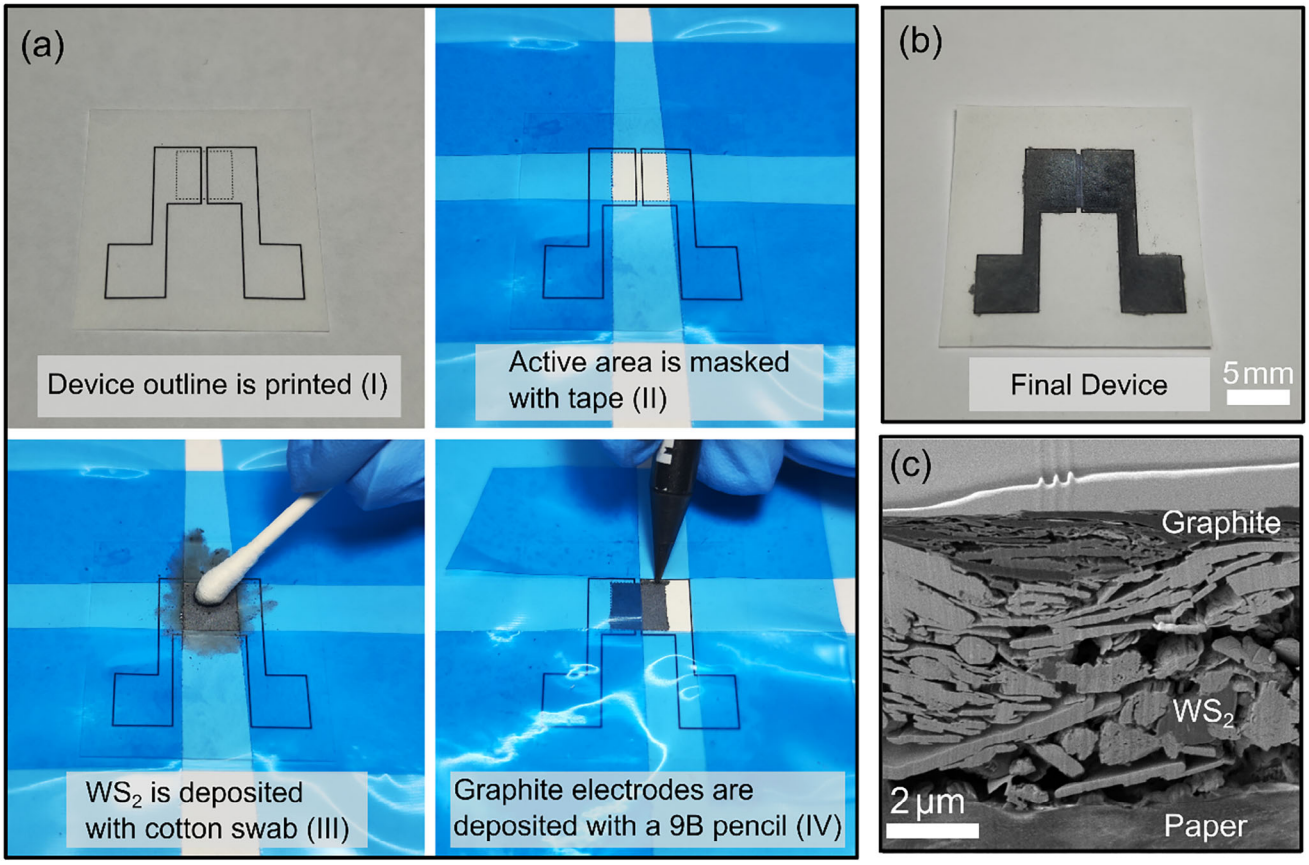

Figure 1. WS_2 Photodetector on water-soluble paper. a) Process sequence of paper-based photodetector device fabrication by abrasion of WS_2 powder and drawing the electrodes using a 9B graphite pencil. b) A photograph of the fabricated WS_2 photodetector device, c) Cross-sectional SEM images of WS_2 flakes deposited on water-soluble paper, illustrating the integration of WS_2 with graphite electrodes.

focused on organic or polymeric active materials with limited environmental stability and spectral tunability. Here, WS_2 is selected as a photoactive material due to its high optical absorption in the visible range, and excellent photoconductive properties. Graphite is chosen as the electrode material for its high electrical conductivity and compatibility with paper-based substrates, while also offering an eco-friendly alternative to metal electrodes, aligning with the sustainability goal of this work. By integration of these materials on a water-soluble paper substrate, we enable a high-performance, and eco-friendly photodetector along with the possibility of recycling the materials. The device demonstrates high and reproducible photoresponse. The significant improvement in photoresponse has been achieved by increasing incident light power and by applying a high bias voltage. Moreover, we show that the device can be completely dissolved in water in 60 s, and the electronic materials (electrodes and semiconductor channel) can be recovered by vacuum filtering. This capability paves the way for future research exploring the reusability of recovered materials, potentially enhancing the sustainability of transient electronics. Taking advantage of these superior properties, developing paper-based transient photodetectors seems to be not only a cost-effective solution but also offers environmentally friendly and disposable functionalities.

2. Results and Discussion

Figure 1a shows the preparation process of the water-soluble WS_2 photodetector. The device fabrication begins with the printing of the outline using an office printer (Brother MFCL5700DN) on soluble paper (Jaboneko, 0.55 g cm^{-3}), which is made of sodium methyl carboxyl cellulose and wood pulp. Then, the channel area is delimited by using Nitto tape (SPV 224) to create stencils and control the geometry of the deposited films. WS_2 powder (0.6 µm APS Micronized, HAGEN Automation,) is rubbed against the unmasked surface of the paper with a cotton swab. This abrasion process applies lateral shear forces to the layered WS_2 powder, promoting the exfoliation and deposition of few-layer flakes. The rough and porous texture of the paper surface improves the adhesion of the flakes, leading to the formation of a continuous and electrically connected network without the use of solvents or binders.

To verify the quality of the film, a handheld multimeter is used, and the rubbing process is repeated until a resistance between two probes separated by ≈1–2 mm reaches a range of ≈1–5 MΩ. This resistance range is used as a threshold to verify uniform deposition and reliable electrical contact in each device. Following this, the masking tape is removed, and the graphite electrodes are drawn with 9B pencil (Monolith, 20409) onto WS_2 and the

printed electrode outline. The completed WS_2 photodetector device is shown in Figure 1b, demonstrating the effective integration of WS_2 on water-soluble paper and confirming the viability of the production technique.

A cross-sectional scanning electron microscopy (SEM) image demonstrates a microscopic view of the WS_2 flakes formed on the water-soluble paper and the integration of the graphite electrodes into the device (Figure 1c). The graphite electrode and WS_2 film can be distinguished due to their difference in material properties under SEM analysis. As can be seen, the WS_2 nanosheets form a network of flakes interconnected through junctions.[29,30] Additionally, we analyzed the thickness of the WS_2 flakes forming the film, finding the modal value of 116 ± 5 nm but exhibiting a significant thickness variation throughout the film, due to the fibrous structure of the paper (Figure S1, Supporting Information).

The photodetection performance of the fabricated WS_2 device is studied using a homebuilt probe station with a source-measure unit (Keithley 2450) under dark and light illumination of an external 660 nm wavelength LED (Thorlabs fiber-coupled LEDs).[31] **Figure 2a** shows the photocurrent-time characteristics of the device while the illumination is switched periodically ON and OFF at a fixed power density of 1.63 mW cm^{-2} (at 5 V bias). The current demonstrates an increase upon illumination and returns to the initial dark current value when the light source is turned off, the device exhibits consistent and reversible switching behavior under 125 on/off cycles (Figure S2, Supporting Information).

The transient photoresponse under excitation of different incident power intensities (from 0.18 to 1.63 mW cm^{-2}), as shown in Figure 2b, shows a gradual increase of photocurrent with the increment of incident power (the baseline has been subtracted to enable quantitative comparison). As the intensity of the incident light increases, more photons interact with the WS_2 film, generating an increased number of electron–hole pairs. This increased generation of charge carriers allows more charge carriers to contribute to the current, resulting in a higher photoresponse.[32] Additionally, by increasing the excitation power, the response time becomes shorter due to faster charge carrier generation and recombination (Figure S3, Supporting Information).[33,34]

Figure 2c shows the extracted photocurrent and responsivity values (obtained from Figure 2b) as a function of the incident light power. At high illumination power, an increase in photocurrent is observed. To quantify this increase, the photocurrent for different incident power regimes is plotted (Figure S4, Supporting Information) and fitted by the power-law:

$$I_{PC} = A \times P^{\alpha} \quad (1)$$

where I_{PC} is the photocurrent and A as well as α are fitting parameters. The photocurrent follows a sub-linear trend with $\alpha \approx 0.5 \pm 0.04$ under lower incident power (< 1 mW cm^{-2}), suggesting the involvement of trap-mediated transport mechanisms (Figure S4a, Supporting Information).[35,36]

To explore this further, we estimated the photoconductive gain *G*, defined as the number of carriers collected per absorbed photon. Surprisingly, the extracted gain values were very low, in the order of 10^{-5} (Figure S5, Supporting Information). This value is several orders of magnitude lower than typical for photogating-dominated devices, which often exhibit high gain due to

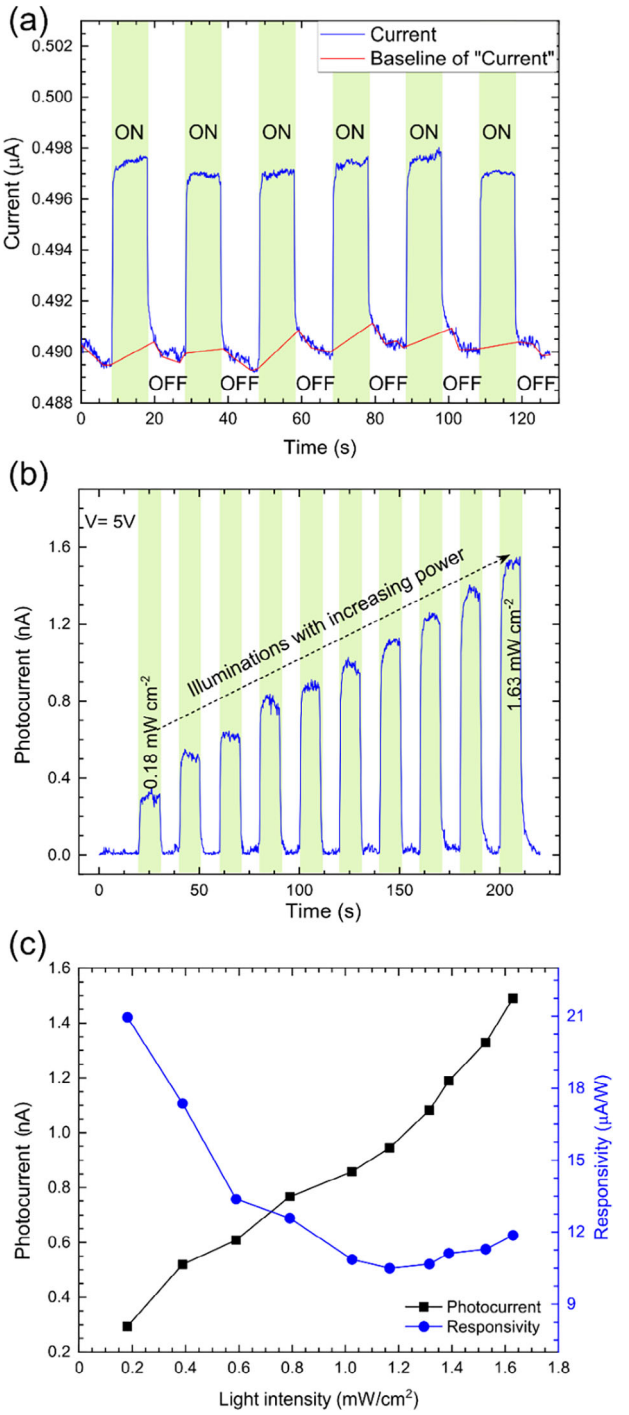

Figure 2. Photoresponse characteristics of the WS_2 photodetector on water-soluble paper. a) Time-resolved photocurrent response under periodic illumination switching at 5 V bias voltage (the red line marks the baseline of the spectrum) b) Photocurrent versus time curve (after subtraction of the baseline) under different incident light intensities at 5 V bias voltage, c) Photocurrent (left) and responsivity (right) as functions of light power density. Measurements are taken at a bias of 5 V and under 660 nm light illumination. The device features a channel width of ≈0.8 mm and a length of 8.8 mm.

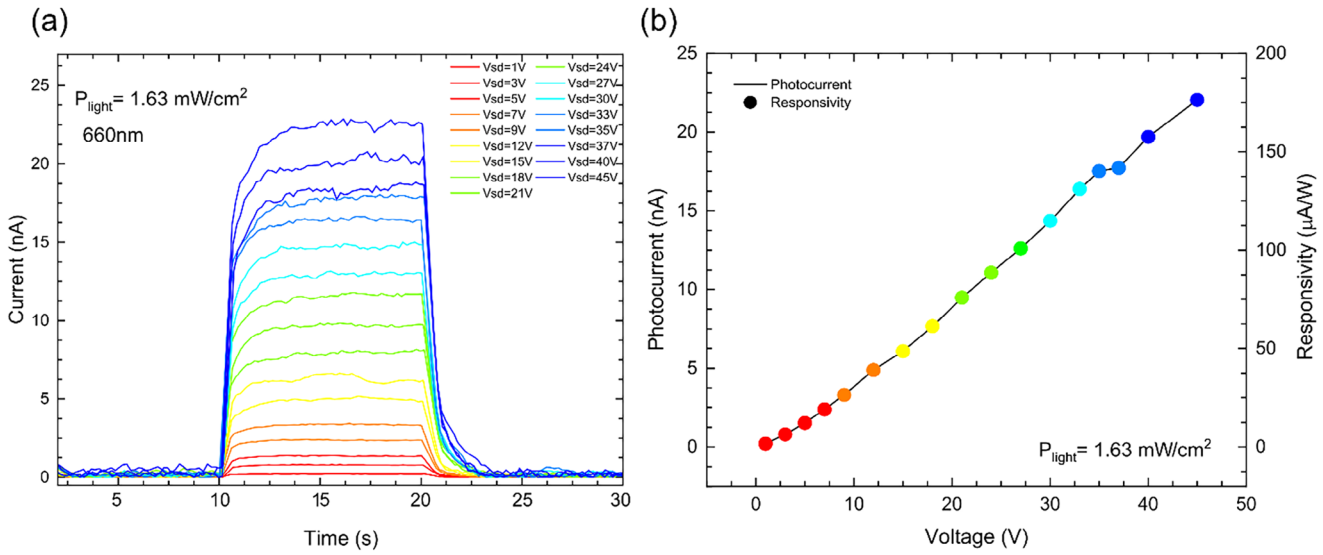

Figure 3. Voltage dependence of photocurrent generation in WS_2 photodetectors. a) Photocurrent response ON-OFF behavior of the photodetector under different bias voltages. b) Voltage-dependent photocurrent and responsivity of the device at fixed power of 0.7 mW. NOTE: Measurements are taken at a wavelength of 660 nm.

long-lived trapped carriers. This suggests that while trap states (e.g., sulfur vacancies, edge defects) may influence transport at low power, the photogating contribution is limited or not efficient in this device architecture. Instead, the sublinear regime may reflect a combination of defect-limited photoconduction and carrier recombination dynamics, where the density of photogenerated carriers is constrained by finite lifetimes or inefficient charge separation.

As the light intensity increases, trap states may saturate, and the photocurrent shows a transition to superlinear behavior with $\alpha \approx 1.37 \pm 0.06$, consistent with thermal-assisted effects such as the photothermoelectric or bolometric response. These mechanisms are known to dominate in 2D materials on insulating or rough substrates and can lead to strong enhancement in photocurrent under high power illumination.[37–39]

We further studied the response of the device to different bias voltages at a fixed wavelength (660 nm). The current dramatically increases upon light on and drops after the light is switched off (**Figure 3a**), which is also verified with current-time characteristics in Figure S6 (Supporting Information) under different light power. The responsivity and photocurrent are compared at fixed light power intensity of 1.63 mW cm^{-2} (660 nm) under different biases (Figure 3b). Both photocurrent and responsivity increase gradually as the applied voltage increases, from ≈0.21 nA and ≈1.68 μAW^{-1}, reaching ≈22 nA, and ≈176 μAW^{-1}, respectively.

The voltage-dependent behavior illustrates that the device's photocurrent and responsivity can be modulated through bias, enabling tunable sensitivity for different application requirements. The steady increase in performance with bias suggests efficient transport across the WS_2 channel and minimal barriers at the graphite-WS_2 interface. However, high operating voltages, such as 45 V, may be impractical for low-power or wearable electronics. To address this, we fabricated an additional device with reduced electrode spacing, which achieved comparable photocurrent at a significantly lower bias. As shown in Figure S7 (Supporting Information) this device achieved a similar performance at 18 V, demonstrating that operational voltage can be effectively minimized through geometric optimization.

The photoresponse of the paper-based photodetector is further examined under various wavelengths, ranging from 470 to 740 nm, at constant intensity of 0.70 $mWcm^{-2}$ (Figure S8, Supporting Information). The fabricated device exhibits a good broad spectral response from 470 to 740 nm with the peak sensitivity located at 660 nm. This behavior can be attributed to the intrinsic optical absorption properties of WS_2, which typically shows a prominent A-exciton absorption peak in the 620–660 nm range due to direct transitions at the K-point of the Brillouin zone.[40,41] The thickness of the abraded WS_2 layer may affect absorption efficiency at the spectral edges. Additionally, the responsivity increases with the wavelength and exhibits a higher response (83 μAW^{-1}) under the illumination of a 660 nm monochromatic light.

The stability of the device under ambient conditions was evaluated over a 24-h period. As shown in Figure S9 (Supporting Information) the photocurrent gradually decreased from ≈7 μA at 0 h to ≈1.35 μA after one day. This decline is likely due to moisture absorption or gradual degradation of the paper substrate. Although the performance decreased over time, the device remained operational, supporting its suitability for sensing or disposable electronics applications.

To evaluate the mechanical durability of the WS_2 photodetector, the electrical response is measured under different applied strains. The I-V characteristics under different strain levels (0–0.44%) are shown in Figure S10 (Supporting Information). The results demonstrate a consistent and nearly linear behavior across all strain conditions, indicating that the electrical contacts remain stable under deformation, and the charge transport within the device is preserved. Furthermore, gauge factor (GF) is extracted from the relative resistance change ($\Delta R/R_0$) as a function of strain, resulting in values of 32.7 and 31.9 for bias voltages of −5V and +5V, respectively. These values indicate that the

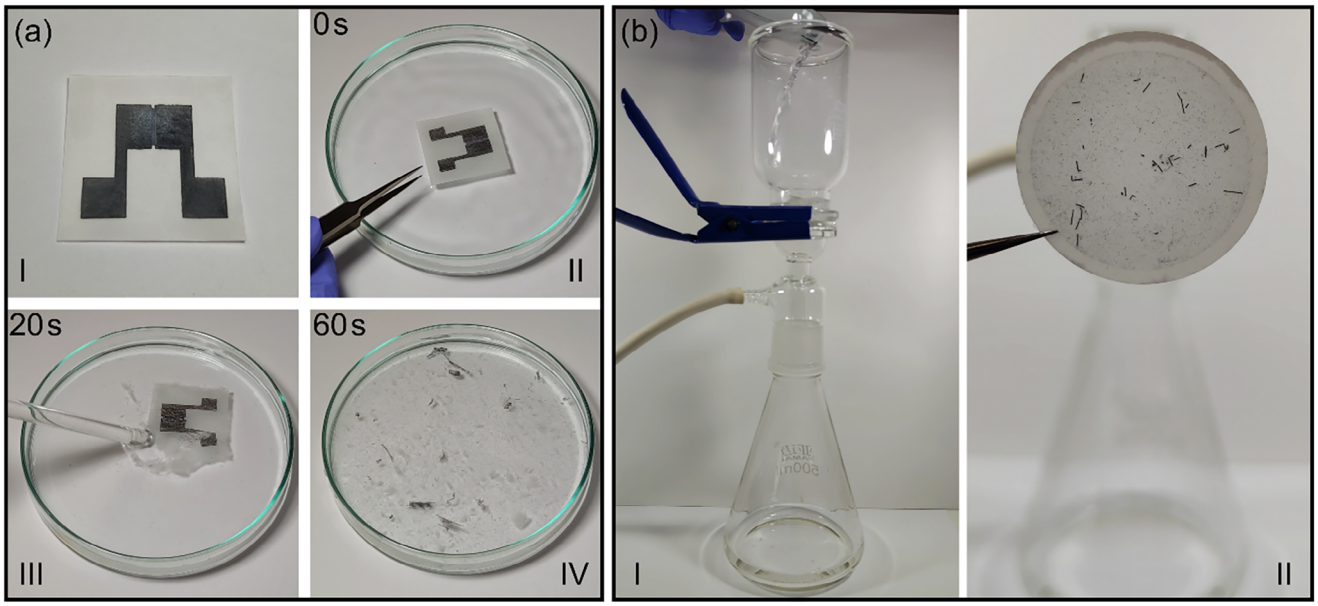

Figure 4. Recycling of WS_2 photodetector. a) Images of the dissolving process steps of paper-based WS_2 photodetector in DI water. b) Vacuum filtering process of the dissolved device, illustrating the recovered materials.

device can effectively maintain its performance under mechanical deformations. In addition to single-cycle strain measurements, we examined the mechanical durability of the device through repeated bending. The device was subjected to 30 strain-release cycles, and resistance values were extracted from I–V measurements taken at each cycle. The change in resistance ($\Delta R/R_n$) increased slightly over time (Figure S10c, Supporting Information). Despite this, the device maintained stable operation throughout the test, confirming its mechanical stability and suitability for flexible electronics applications.

Additional I–V measurements were carried out under 660 nm illumination while the device was subjected to different strain levels (Figure S11, Supporting Information). Similar to the dark condition, the I–V curves remained linear under strain, and the device continued to show stable electrical behavior. These results suggest that the photoresponse of the device is not significantly affected by mechanical strain.

To demonstrate the degradability of the fabricated photodetector, the device is placed into de-ionized (DI) water at room temperature. **Figure** 4a shows a series of captured images demonstrating the dissolution process. The process consists of three steps: water absorption, disintegration, and dissolution. In the first step, the device immediately absorbs the water, and subsequently, the substrate starts to disintegrate. In 60 s, the device substrate disappears while the other elements of the device remain suspended in the water. Moreover, the materials used for device fabrication are collected by using a vacuum filtration method based on cellulose filter paper (prat dumas, 47 mm) with 0.20 µm pore size (Figure 4b). Since WS_2 is chemically stable in water and does not dissolve under ambient conditions, it remains suspended along with other non-soluble components after the substrate disintegrates. This is because WS_2 has a layered structure, where tungsten (W) atoms are covalently bonded to sulfur (S) atoms, making it resistant to interaction with water molecules due to its high bond energy and the hydrophobic nature of its sulfur-terminated surfaces.[42,43] Therefore, the vacuum filtration process efficiently separates these materials from the solution, enabling their recovery for potential reuse. We address the reader to a video that shows the overall dissolving process (see Video S1, Supporting Information).

Several previous studies have explored the use of pencil-based or solution-processed materials for low-cost photodetector fabrication on paper substrates. However, these approaches typically lack transient behavior, employ non-dissolvable substrates, or do not consider recyclability. In comparison, the device reported in this work integrates WS_2 as the photoactive material and graphite electrodes on a fully water-soluble paper substrate, using a completely dry, solvent-free fabrication process. This combination enables not only rapid disintegration under ambient conditions but also the recovery of functional materials after-use. A comparative overview of recent works on paper-based and transient photodetectors is presented in Table S1 (Supporting Information).

Furthermore, we investigate whether the recovered materials remain unaltered by the recycling process, opening the door for reusing them in the future. Raman spectroscopy measurements are taken to identify the recovered materials' properties (laser wavelength of 532 nm). The Raman spectra of WS_2 on soluble and filter paper are shown in Figure S12 (Supporting Information). Abraded WS_2 on soluble paper exhibits characteristic modes E^1_{2g} and A_{1g} appearing at 346 and 419 $cm\_^1$ respectively. These peaks serve as spectral fingerprints, confirming the presence of WS_2 on paper. The collected Raman spectrum from filter paper provides two significant outcomes to comprehensively understand the material after the dissolution process. Spectrum 1 obtained from large bulk area (Figure S12b, Supporting Information) distinctly exhibits the characteristic WS_2 Raman peaks. On the other hand, spectrum 2 demonstrates a mix of WS_2 and graphite. These results are also consistent with the

Energy-Dispersive X-ray Spectroscopy (EDX) results. The EDX spectrum indicates the presence of elements W and S in the films, which confirms the presence of WS_2 before and after filtration (Figure S13, Supporting Information).

In addition to demonstrating the transient behavior of our devices, we conducted a proof-of-concept experiment to explore the potential for material reuse following substrate dissolution. To isolate the active material, we first fabricated a WS_2 film on water-soluble paper, which was then dissolved in water to release the WS_2. The resulting dispersion was filtered and dried, and the recovered WS_2 was reused to fabricate a second device using the same dry abrasion method, combined with freshly drawn graphite electrodes (see Figure S14a, Supporting Information). As shown in Figure S14 (Supporting Information), the recycled device exhibited a stable photocurrent response under increasing illumination power. While the overall performance was lower than that of the original device, likely due to material loss or aggregation during the recovery process, the experiment confirms that the recovered WS_2 retains sufficient optoelectronic functionality for reuse. This supports the viability of circular fabrication strategies and highlights the relevance of transient electronics for advancing sustainable materials design.

We note that in the full device architecture, WS_2 and graphite would be recovered as a mixed material. While we foresee that techniques such as cascade centrifugation could, in principle, enable the separation of components based on size and density differences, developing an efficient, scalable separation protocol is a substantial undertaking beyond the current scope. Our current experiment was designed as a minimal, yet realistic, demonstration of the concept's viability. We believe it offers a strong foundation for future work on full-material recovery cycles.

3. Conclusion

In summary, we successfully demonstrated a flexible, cost-effective transient photodetector consisting of abraded WS_2 as an active channel, pencil-drawing graphite as electrodes, and water-soluble paper as the device substrate. The as-fabricated devices exhibit reversible response upon light illumination cycles. Moreover, the responsivity can be improved by applying a higher bias voltage, achieving a maximum of 176 μAW^{-1} at an applied voltage of 45 V. Finally, we demonstrated that the detector can be fully dissolved in water within a minute.

This work demonstrates the potential of soluble WS_2 transient photodetectors, offering a valuable step toward addressing the growing challenge of electronic waste. Overall, we believe that our findings greatly expand new possibilities for electronic applications, such as disposable environmental sensors, transient biomedical diagnostics, and short-term security systems, not only reducing their cost but also minimizing e-waste to address global environmental concerns. Furthermore, our work highlights the economic contribution of transient technologies by enabling the recovery of materials that might be reused in other processes or devices.

Supporting Information

Supporting Information is available from the Wiley Online Library or from the author.

Acknowledgements

A.C-G. acknowledges funding by the Ministry of Science and Innovation (Spain) through the projects TED2021-132267B-I00, PID2020-115566RB-I00, PDC2023-145920-I00, and PID2023-151946OB-I00 and the European Research Council through the ERC-2024-PoC StEnSo (grant agreement 101185235) and the ERC-2024-SyG SKIN2DTRONICS (grant agreement 101167218). G.E. acknowledges the Ministry of Education of Turkey for the YLSY Scholarship Program. L.D. appreciates support from Science Foundation Ireland (SFI) (18/EPSRC-CDT/3581) and availed of the facilities of the SFI-funded advanced microscopy laboratory (AML). J.N.C. appreciates support from the SFI-funded centre AMBER (SFI/12/RC/2278).

Conflict of Interest

The authors declare no conflict of interest.

Data Availability Statement

The data that support the findings of this study are available from the corresponding author upon reasonable request.

Keywords

transient electronics, paper electronics, photodetector, van der Waals materials, tungsten disulfide

Received: April 15, 2025
Revised: July 1, 2025
Published online: July 23, 2025

[1] A. R. K. Gollakota, S. Gautam, C. M. Shu, *J. Environ. Manage.* **2020**, *261*, 110234.
[2] J. S. Shim, J. A. Rogers, S. K. Kang, *Mater. Sci. Eng. R Rep.* **2021**, *145*, 100624.
[3] P. Kiddee, R. Naidu, M. H. Wong, *Waste Manag.* **2013**, *33*, 1237.
[4] M. Monisha, S. Agarwala, *Mater Sci Addit Manuf* **2022**, *1*, 15.
[5] S. Himalyan, V. Gupta, *Qual Quant.* **2024**, *58*, 3559.
[6] S.-W. Hwang, D.-H. Kim, H. Tao, T.-i. Kim, S. Kim, K .J. Yu, B. Panilaitis, J.-W. Jeong, J.-K. Song, F .G. Omenetto, J. A. Rogers, *Adv. Funct. Mater.* **2013**, *23*, 4087.
[7] D. Tobjörk, R. Österbacka, *Adv. Mater.*. **2011**, *23*, 1935.
[8] T. Kaneko, T. H. Thi, D. J. Shi, M. Akashi, *Nat. Mater.* **2006**, *5*, 966.
[9] D.-H. Kim, Y.-S. Kim, J. Amsden, B. Panilaitis, D. L. Kaplan, F. G. Omenetto, M. R. Zakin, J. A. Rogers, *Appl. Phys. Lett.* **2009**, *95*, 133701.
[10] Y. Zhou, C. Fuentes-Hernandez, T. M. Khan, J.-C. Liu, J. Hsu, J. W. Shim, A. Dindar, J. P. Youngblood, R. J. Moon, B. Kippelen, *Sci. Rep.* **2013**, *3*, 1536.
[11] C. J. Bettinger, Z. Bao, *Adv. Mater.* **2010**, *22*, 651.
[12] S.-W. Hwang, G. Park, H. Cheng, J.-K. Song, S.-K. Kang, L. Yin, J.-H. Kim, F. G. Omenetto, Y. Huang, K. Lee, J. A. Rogers, *Adv. Mater.* **2014**, *26*, 1992.
[13] L. Yin, A. B. Farimani, K. Min, N. Vishal, J. Lam, Y. K. Lee, N. R. Aluru, J. A. Rogers, *Adv. Mater.* **2015**, *27*, 1857.
[14] F. Eder, H. Klauk, M. Halik, U. Zschieschang, G. Schmid, C. Dehm, *Appl. Phys. Lett.* **2004**, *84*, 2673.
[15] N. Mittal, A. Ojanguren, M. Niederberger, E. Lizundia, *Adv. Sci.* **2021**, *8*, 2004814.
[16] S.-W. Hwang, H. Tao, D.-H. Kim, H. Cheng, J.-K. Song, E. Rill, M. A. Brenckle, B. Panilaitis, S. M. Won, Y.-S. Kim, Y. M. Song, K. J. Yu, A.

Ameen, R. Li, Y. Su, M. Yang, D. L. Kaplan, M. R. Zakin, M. J. Slepian, Y. Huang, F. G. Omenetto, J. A. Rogers, *Science* **2012**, *337*, 1640.
[17] X. Jia, C. Wang, V. Ranganathan, B. Napier, C. Yu, Y. Chao, M. Forsyth, F. G. Omenetto, D. R. MacFarlane, G. G. Wallace, *ACS Energy Lett.* **2017**, *2*, 831.
[18] C. W. Park, S.-K. Kang, H. L. Hernandez, J. A. Kaitz, D. S. Wie, J. Shin, O. P. Lee, N. R. Sottos, J. S. Moore, J. A. Rogers, S. R. White, *Adv. Mater.* **2015**, *27*, 3783.
[19] K. K. Fu, Z. Wang, J. Dai, M. Carter, L. Hu, *Chem Mater.* **2016**, *28*, 3527.
[20] H. Cheng, V. Vepachedu, *Theor Appl Mech Lett* **2016**, *6*, 21.
[21] K. J. Yu, D. Kuzum, S.-W. Hwang, B. H. Kim, H. Juul, N. H. Kim, S. M. Won, K. Chiang, M. Trumpis, A. G. Richardson, H. Cheng, H. Fang, M. Thompson, H. Bink, D. Talos, K. J. Seo, H. N. Lee, S.-K. Kang, J.-H. Kim, J. Y. Lee, Y. Huang, F. E. Jensen, M. A. Dichter, T. H. Lucas, J. Viventi, B. Litt, J. A. Rogers, *Nat. Mater.* **2016**, *15*, 782.
[22] C. H. Lee, H. Kim, D. V. Harburg, G. Park, Y. Ma, T. Pan, J. S. Kim, N. Y. Lee, B. H. Kim, K. Jang, S.-K. Kang, Y. Huang, J. Kim, K. Lee, C. Leal, J. A. Rogers, *NPG Asia Mater* **2015**, *7*, 227.
[23] S.-K. Kang, R. K. J. Murphy, S.-W. Hwang, S. M. Lee, D. V. Harburg, N. A. Krueger, J. Shin, P. Gamble, H. Cheng, S. Yu, Z. Liu, J. G. McCall, M. Stephen, H. Ying, J. Kim, G. Park, R. C. Webb, C. H. Lee, S. Chung, D. S. Wie, A. D. Gujar, B. Vemulapalli, A. H. Kim, K. Lee, J. Cheng, Y. Huang, S. H. Lee, P. V. Braun, W. Z. Ray, J. A. Rogers, *Nature* **2016**, *530*, 71.
[24] G. A. Salvatore, J. Sülzle, F. Dalla Valle, G. Cantarella, F. Robotti, P. Jokic, S. Knobelspies, A. Daus, L. Büthe, L. Petti, N. Kirchgessner, R. Hopf, M. Magno, G. Tröster, *Adv. Funct. Mater.* **2017**, *27*, 1702390.
[25] W. B. Han, J. H. Lee, J. W. Shin, S. W. Hwang, *Adv. Mater.* **2020**, *32*, 2002211.
[26] R. Li, L. Wang, D. Kong, L. Yin, *Bioact Mater* **2018**, *3*, 322.
[27] H. L. Hernandez, S.-K. Kang, O. P. Lee, S.-W. Hwang, J. A. Kaitz, B. Inci, C. W. Park, S. Chung, N. R. Sottos, J. S. Moore, J. A. Rogers, S. R. White, *Adv. Mater.* **2014**, *26*, 7637.
[28] S. S. Pandey, N. Banerjee, Y. Xie, C. H. Mastrangelo, *Adv. Mater. Technol.* **2018**, *3*, 1800044.
[29] A. G. Kelly, D. O'Suilleabhain, C. Gabbett, J. N. Coleman, *Nat. Rev. Mater.* **2022**, *7*, 217.
[30] S. Barwich, A. Rafferty, M. S. Ferreira, J. N. Coleman, *Carbon* **2021**, *171*, 306.
[31] J. Quereda, Q. Zhao, E. Diez, R. Frisenda, A. Castellanos-Gomez, *Open Res Eur* **2022**, *1*, 98.
[32] D. Gross, I. Mora-Seró, T. Dittrich, A. Belaidi, C. Mauser, A. J. Houtepen, E. D. Como, A. L. Rogach, J. Feldmann, *J. Am. Chem. Soc.* **2010**, *132*, 5981.
[33] C. Labanti, J. Wu, J. Shin, S. Limbu, S. Yun, F. Fang, S. Y. Park, C.-J. Heo, Y. Lim, T. Choi, H. Kim, H. Hong, B. Choi, K.-B. Park, J. R. Durrant, J. Kim, *Nat. Commun.* **2022**, *13*, 3745.
[34] S. Guo, X. Zhao, Y. He, Z. Pan, M. Yang, Y. Cai, "Low-Voltage and High-Gain Ultraviolet Detector Based on 4H-SiC n-p-n Bipolar Phototransistor," in IEEE Transactions on Electron Devices **2021**, *68*, pp. 2342–2346,
[35] M. Buscema, J. O. Island, D. J. Groenendijk, S. I. Blanter, G. A. Steele, H. S. J. van der Zant, A. Castellanos-Gomez, *Chem. Soc. Rev.* **2015**, *44*, 3691.
[36] J. O. Island, S. I. Blanter, M. Buscema, H. S. J. van der Zant, A. Castellanos-Gomez, *Nano Lett.* **2015**, *15*, 7853.
[37] Y. Zhang, H. Li, L. Wang, H. Wang, X. Xie, S. Zhang, R. Liu, Z.-J. Qiu, *Sci. Rep.* **2015**, *5*, 7938.
[38] D. Vaquero, V. Clericò, J. Salvador-Sánchez, E. Díaz, F. Domínguez-Adame, L. Chico, Y. M. Meziani, E. Diez, J. Quereda, *Nanoscale* **2021**, *13*, 16156.
[39] M. Freitag, T. Low, F. Xia, P. Avouris, *Nat. Photonics* **2013**, *7*, 53.
[40] W. Zhao, Z. Ghorannevis, L. Chu, M. Toh, C. Kloc, P.-H. Tan, G. Eda, *ACS Nano* **2013**, *7*, 791.
[41] L. Zeng, L. Tao, C. Tang, B. Zhou, H. Long, Y. Chai, S. P. Lau, Y. H. Tsang, *Sci. Rep.* **2016**, *6*, 20343.
[42] H. Song, X. Yu, M. Chen, M. Qiao, T. Wang, J. Zhang, Y. Liu, P. Liu, X. Wang, *Appl. Surf. Sci.* **2018**, *439*, 240.
[43] N. Li, J. Su, Z. Xu, D. P. Li, Z. T. Liu, *J. Phys. Chem. Solids* **2016**, *89*, 84.